Journal of Power Sources 243 (2013) 172–180

Contents lists available at SciVerse ScienceDirect

Journal of Power Sources

journal homepage: www.elsevier.com/locate/jpowsour

Characterization of Ni–YSZ anodes for solid oxide fuel cells fabricated by suspension plasma spraying with axial feedstock injection

Craig Metcalfe, Joel Kuhn, Olivera Kesler*

University of Toronto, Department of Mechanical and Industrial Engineering, 5 King's College Road, Toronto, Ontario M5S 3G8, Canada

HIGHLIGHTS

- Metal supported SOFC fabricated by plasma spraying with axial feedstock injection.
- Power density of 0.56 W cm^{-2} at 0.7 V was obtained at 750 °C.
- Process parameter and feedstock property effects on anode composition investigated.
- Process parameter and feedstock property effects on anode microstructure investigated.

ARTICLE INFO

Article history:
Received 30 January 2013
Received in revised form
15 May 2013
Accepted 23 May 2013
Available online 10 June 2013

Keywords:
Solid oxide fuel cell (SOFC)
Nickel–yttria stabilized zirconia (Ni–YSZ)
Suspension plasma spraying (SPS)
Axial injection

ABSTRACT

Composite Ni–$Y_{0.15}Zr_{0.85}O_{1.925}$ anodes were fabricated by axial-injection suspension plasma spraying in open atmosphere conditions. The composition of the anode is controllable by adjustment of the plasma gas composition, stand-off distance, and suspension feed rate. The total porosity is controllable through the addition of carbon black to the suspension as a sacrificial pore-forming material as well as by adjustment of the suspension feed rate. The size of the NiO particles in suspension affects both the composition and total porosity, with larger NiO particles leading to increased Ni content and porosity in the deposited coatings. The surface roughness increases with a decrease of the in-flight droplet momentum, which results from both smaller NiO particles in suspension and the addition of low density pore-forming materials. A solid oxide fuel cell was fabricated with both electrodes and electrolyte fabricated by axial-injection plasma spraying. Peak power densities of 0.718 W cm^{-2} and 1.13 W cm^{-2} at 750 °C and 850 °C, respectively, were achieved.

1. Introduction

Plasma spray processing of solid oxide fuel cell (SOFC) components has the potential to realize several cost and performance benefits over traditional wet ceramic processing techniques [1]. The cost benefits of plasma spray processing include, in part, the elimination of high-temperature sintering steps, which are required for colloidal and wet-chemistry methods. These methods are difficult to implement in metal-supported SOFCs without oxidizing and densifying the metal substrate [2–4]. In addition to process cost reduction, the absence of high-temperature firing steps leads to greater flexibility in the materials that may be used for the electrodes and electrolyte, without inter-reaction between cell layers leading to the formation of non-electrically conductive phases.

There are, however, several challenges to obtaining high-performance SOFCs fabricated by plasma spray methods. These challenges are largely related to obtaining a dense and defect free electrolyte and to obtaining sufficiently porous electrode microstructures having a high density of reaction sites. Significant progress has been made to address these issues by researchers at the German Aerospace Centre (DLR) [5,6], Forschungszentrum Jülich [7,8], and the National Research Council of Canada [9,10].

To obtain a high density of reaction sites, composite Ni–YSZ anodes require small feature sizes and uniform mixing of the Ni and YSZ phases. Conventional atmospheric plasma spraying makes use of dry powder feedstock. These feedstocks consist of agglomerates between approximately 10 μm and 100 μm in diameter. The agglomerates may have primary particles on the order of tens of nanometers [11,12]; however, the deposited coatings are generally described as having a bi-modal microstructure. This structure results from the outer region of the agglomerate being melted in-flight, while the inner region of the agglomerate retains its structure [13]. There is potential to fabricate SOFC electrodes having a more

* Corresponding author. Tel.: +1 (416) 978 3835; fax: +1 (416) 978 7753.
E-mail addresses: tcm@mie.utoronto.ca (C. Metcalfe), joel.kuhn@mail.utoronto.ca (J. Kuhn), kesler@mie.utoronto.ca (O. Kesler).

0378-7753/$ – see front matter © 2013 Elsevier B.V. All rights reserved.
http://dx.doi.org/10.1016/j.jpowsour.2013.05.174

uniform fine-scale structure with the use of suspension plasma spraying (SPS) [14,15]. In SPS, feedstock particles having diameters on the sub-micrometer to micrometer size scales are suspended in a liquid and subsequently injected into the plasma jet [16].

The deposition of porous Ni–YSZ anodes having a high density of reaction sites by SPS requires control of several processing parameters, which affect the resulting coating composition and microstructure. For SPS processes involving radial injection of the suspension, *e.g.* Refs. [17,18], injection parameters must be controlled to produce the required droplet velocity and size distributions to penetrate the plasma jet. A lesser degree of control is required for axial feedstock injection, in which the suspension is injected directly into the core of the plasma jet. Processing parameters such as total plasma gas flow rate, stand-off distance, and suspension feed rate have been identified as being critical factors controlling the coating porosity and deposition rate for axial injection of suspension [19]. Properties of the suspension feedstock include surface tension and viscosity, which are in part determined by the dispersion medium used (*e.g.* water or alcohol). Alcohol based suspensions have shown promise toward the fabrication of coatings having higher porosity compared to those fabricated using aqueous suspensions [18,20].

In this work, axial injection SPS has been used to deposit NiO–YSZ coatings to determine the effect of plasma processing conditions and feedstock properties on the deposition efficiency (DE) and coating properties including composition, total porosity, and surface roughness. The plasma processing parameters of interest were the plasma gas composition and stand-off distance. The feedstock properties included the mass flow rate of the injected NiO–YSZ suspension, NiO particle size, and quantity of sacrificial pore-forming material in suspension. Based upon the observed relationships between plasma processing parameters and coating composition and microstructure, a metal supported SOFC having an anode functional layer fabricated by SPS was characterized electrochemically.

2. Experimental procedure

2.1. Plasma spray processing

The NiO–YSZ coatings were deposited using an axial injection atmospheric plasma spray (APS) system (Axial III Series 600, Northwest Mettech Corp., North Vancouver, BC, Canada). Porous 430 stainless steel discs (Mott Corporation, Farmington, CT, USA) having a diameter of 25.4 mm and thickness of 1.6 mm were used as supports, unless otherwise indicated. Prior to anode and cathode coating deposition, the supports were mounted on an active heating and cooling device, which uses air as the working fluid. The supports were preheated to approximately 250 °C and cooled with air when the back surface of the substrate reached 400 °C. The plasma torch was rastered over the substrates at a speed of 63.5 cm s^{-1}. The electrolyte was deposited as described in Ref. [12].

The suspension was delivered to the torch using a suspension delivery system (Northwest Mettech Corp., North Vancouver, BC, Canada) equipped with a peristaltic pump, Coriolis mass flow meter, and downstream pulse dampener. The suspension was axially injected into the plasma through a syringe tube having an internal diameter of 0.84 mm. Nitrogen at 20 slpm was used as an atomizing gas. With this system, good control of the mass flow rate of suspension is obtained. At a set point of 50 g min^{-1}, the actual flow rate varied between 49 g min^{-1} and 51 g min^{-1}, where the variation was due to pulsations introduced by the peristaltic pump.

For fabrication of fuel cells, a bi-layer anode was fabricated, which was deposited directly onto the metal support, followed by the electrolyte and cathode. No other diffusion barrier layers or protective coatings were used. The first layer of the bi-layer anode was deposited using a dry-powder feedstock consisting of nanostructured agglomerates, as detailed in Ref. [12]. The purpose of this layer was to bridge the large surface pores (up to 80 μm in the metal supports used) in order to minimize the surface roughness of the anode, which can adversely affect the quality of the electrolyte. Prior to deposition of the anode functional layer, the bridging layer was lightly sanded by hand with 600 grit sandpaper. After functional layer deposition, the NiO was reduced to Ni and the anode surface was again lightly sanded by hand with 600 grit sandpaper in an attempt to remove sharp asperities. This step reduces the size of the asperities but does not eliminate them. The NiO was reduced to Ni prior to electrolyte deposition to increase the thermal conductivity of the anode, in an attempt to minimize segmentation cracking of the electrolyte [21]. The 60 wt.% $La_{0.6}Sr_{0.4}Co_{0.2}Fe_{0.8}O_{3-\delta}$ (LSCF) and 40 wt.% $Ce_{0.8}Sm_{0.2}O_{1.9}$ (SDC) composite cathode [22], and YSZ electrolyte were deposited using SPS and conventional plasma spraying with nanostructured agglomerated feedstock powder, respectively, as detailed in Ref. [12]. The 25.4 mm diameter button-type fuel cell had an active area of 1 cm^2.

2.1.1. Anode feedstock material

Aqueous suspensions were used in part due to their lower cost compared to alcohol based suspensions and also because the suspension delivery system was not rated for flammable liquids. The NiO and YSZ feedstock powders for the anode functional layer were delivered to the plasma torch as a single aqueous suspension containing both NiO and YSZ powders.

Preparation of the composite suspension involved first making separate suspensions of NiO and of YSZ, and subsequently mixing the two. The NiO suspension was prepared using one or more of three different NiO powders (Type F, Type A, and Type Std., Novamet Specialty Products Corp., Wyckoff, NJ, USA). These NiO powders primarily differ in their particle size distribution, with the Type F, Type A, and Type Std. powders having manufacturer reported d_{50} values of 1–2 μm, 6–10 μm, and 14–18 μm, respectively. The NiO suspensions consisted of 1.5 vol.% NiO using poly(ethyleneimine) (PEI) (Sigma Aldrich, St. Louis, MO, USA) as a dispersant. The YSZ suspension consisted of 2 vol.% $Y_{0.15}Zr_{0.85}O_{1.925}$ powder (Inframat Corporation, Manchester, CT, USA) with PEI as a dispersant.

The separate NiO and YSZ suspensions were subsequently combined such that the volume of suspended solids was 50 vol.% Ni after reduction of NiO to Ni. For coatings fabricated using a sacrificial pore-forming material, carbon black (N991UP, Cancarb Ltd., Medicine Hat, AB, Canada) was added to the composite NiO and YSZ suspension, followed by sonication for 1–3 h as required to break up agglomerates of carbon black particles. The measured particle size distributions for each of the suspended powders used in this work are shown in Fig. 1.

2.1.2. In-flight particle surface temperature measurements

In-flight particle surface temperature measurements were conducted using the DPV-2000 in-flight particle sensor (Tecnar, St-Bruno, QC, CAN). The sensor was centered at the location of highest particle flow rate in order to maximize the count rate of measurable data and to ensure statistical validity of the results. A minimum of 8000 particles were detected for each measurement for constructing the temperature distribution. The in-flight particle surface temperature measurements were used only to compare average particle surface temperatures for two different suspension feed rates. The detection resolution of the sensor depends on both the size of the particle and the intensity of the radiation emitted by the particle. Therefore, to maximize the probability of particle detection, the largest NiO particles (Type Std.), having a d_{50} by volume in suspension of 14 μm, were used.

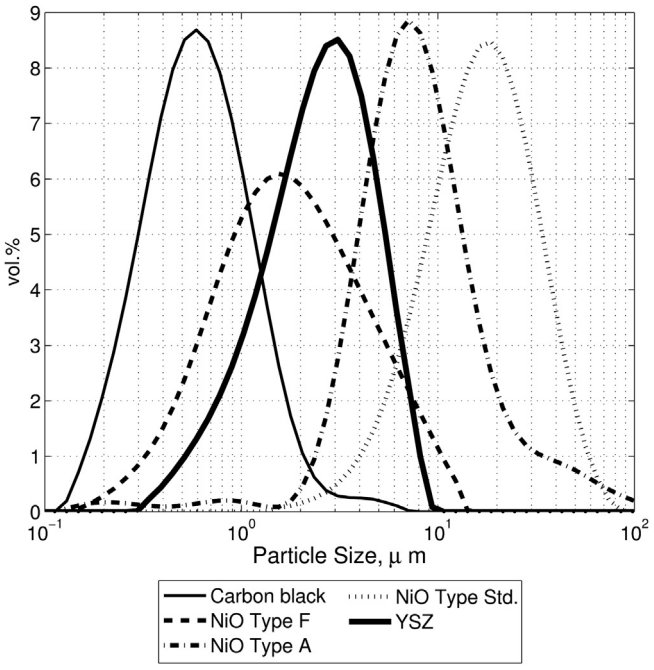

Fig. 1. Particle size distributions for suspensions of three NiO powders: Type F, Type A, and Type Std., as well as suspensions of YSZ and carbon black.

2.2. Anode characterization

2.2.1. Total porosity

Samples for porosity analysis were prepared as described in a previous work [12]. The total porosity was evaluated as the average of two area-normalized regions, each from different backscattered electron images using image analysis software (Clemex Vision PE, Clemex Technologies Inc., Longueuil, QC, Canada). Each image was acquired using a scanning electron microscope (JSM6610, JEOL Ltd, Tokyo, Japan) at a working distance of 11 mm and a magnification of 2500 times using an acceleration voltage of 20 kV.

2.2.2. Composition

The composition of the deposited NiO–YSZ coatings was evaluated for the volume fraction of Ni that would be present after reduction of NiO to Ni, relative to the total solid volume. The coatings were subjected to two different heat treatments. The first heat treatment was at 750 °C for 2 h in air to burn out any pore-forming material and to fully oxidize the NiO. The second heat treatment was at 600 °C for 4 h in a 10 vol.% H_2, balance N_2, atmosphere to reduce the NiO to Ni. The difference in coating masses before and after reduction of NiO to Ni was attributed to the loss of oxygen, after correcting for oxidation of the metal support, and was used to determine the corresponding volume of Ni in the coating.

2.2.3. Deposition efficiency

Deposition efficiency was evaluated by comparing the deposited coating mass to the known feedstock composition and feed rate and torch raster pattern over the substrate. The DE for both NiO and YSZ was obtained by comparing the known composition of the feedstock to the measured Ni content in the deposited coating.

2.2.4. Surface roughness

Average surface roughness values were determined using image analysis techniques. Three backscattered electron images were acquired at 50 times magnification using a working distance of 11 mm and 20 kV acceleration voltage. The average roughness, R_a, in μm, was evaluated over the three images, for a total sample length corresponding to 7.5 mm. At this resolution, each pixel corresponds to a width of 1.0 μm. The substrates used to evaluate surface roughness of the NiO–YSZ coatings were non-porous 430 stainless steel discs having a 25.4 mm diameter and 1.6 mm thickness. The average surface roughness of these discs was 7.2 μm.

2.3. Electrochemical testing

Single cell test stations were developed in-house as described in a previous work [12]. Electrochemical testing was performed using a Solartron 1470E multi-channel potentiostat and a 1260 frequency response analyzer (London Scientific, London, ON, Canada). The oxidant was air (79% N_2, 21% O_2) at a flow rate of 1000 sccm. This high air flow rate was required to maintain the oxygen concentration on the cathode side, which would otherwise be depleted due to combustion with hydrogen that crosses over through defects in the electrolyte. The fuel stream consisted of H_2 with steam additions between 3 mol.% and 25 mol.%. The anode was reduced *in-situ* by increasing the quantity of H_2 until the open circuit voltage (OCV) reached a maximum. The current collectors consisted of 0.4 mm wire diameter gold mesh on both sides of the fuel cell, with the addition of 100 mg of 0.05 mm diameter gold wool between the gold mesh and the cathode to improve current collection.

3. Results and discussion

3.1. Composition of deposited coatings

The difference in melting temperatures between NiO (1980 °C) and YSZ (2700 °C) presents a challenge to the deposition of composite NiO and YSZ anodes. Therefore, an understanding of how plasma processing parameters affect the composition of the deposited coatings is essential for repeatable fabrication of SOFC anodes. The effects of stand-off distance, plasma gas composition, and feed rate of suspension on the Ni content of the deposited coatings were evaluated.

3.1.1. Effect of stand-off distance and plasma gas composition

To understand the effect of stand-off distance and plasma gas composition on deposition of NiO and YSZ, coatings were fabricated using plasma Conditions A, listed in Table 1. Plasma gases containing 40%, 50% and 60% N_2, balance Ar, were used. For each plasma gas composition, standoff distances of 50 mm, 65 mm, and 80 mm were used with a suspension flow rate of 83 g min^{-1}. Type F NiO powder was used for each condition.

Fig. 2(a) shows the vol.% Ni of each deposited coating, relative to total solid volume, as the stand-off distance and plasma gas composition are varied using a total suspension flow rate of 83 g min^{-1}. At this suspension feed rate, the flow rate of NiO is 5.32 g min^{-1} and that of YSZ is 2.86 g min^{-1}. These flow rates

Table 1
Plasma processing condition sets used.

Parameter	Conditions A	Conditions B	Conditions C
Plasma gas flow rate, slpm	225	225	200
vol.% N_2	40, 50, 60	60	60
vol.% Ar	Balance	40	40
Current, A	600	600	600
Arc voltage, V	126, 148, 170	176	168
Torch power, kW	76, 90, 102	106	101
Stand-off distance, mm	50, 65, 80	50	50
Nozzle diameter, mm	9.5	9.5	9.5
Total feedstock flow rate, g min^{-1}	50, 83	83	50, 83

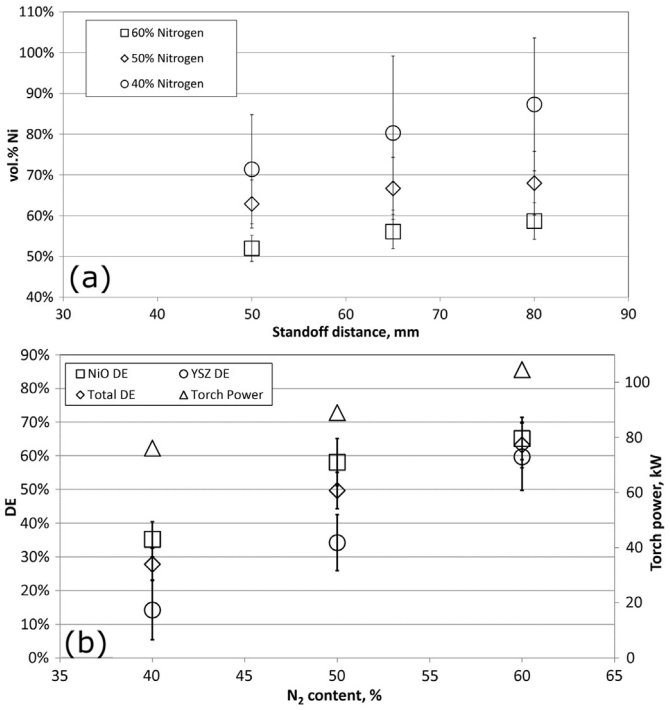

Fig. 2. (a) Nickel volume fraction, relative to total solid volume of Ni and YSZ phases, with increasing stand-off distance for a range of plasma gas compositions. (b) Torch power, total DE, and NiO and YSZ DE at 50 mm stand-off distance for 40%, 50%, and 60% N_2 in the plasma gas.

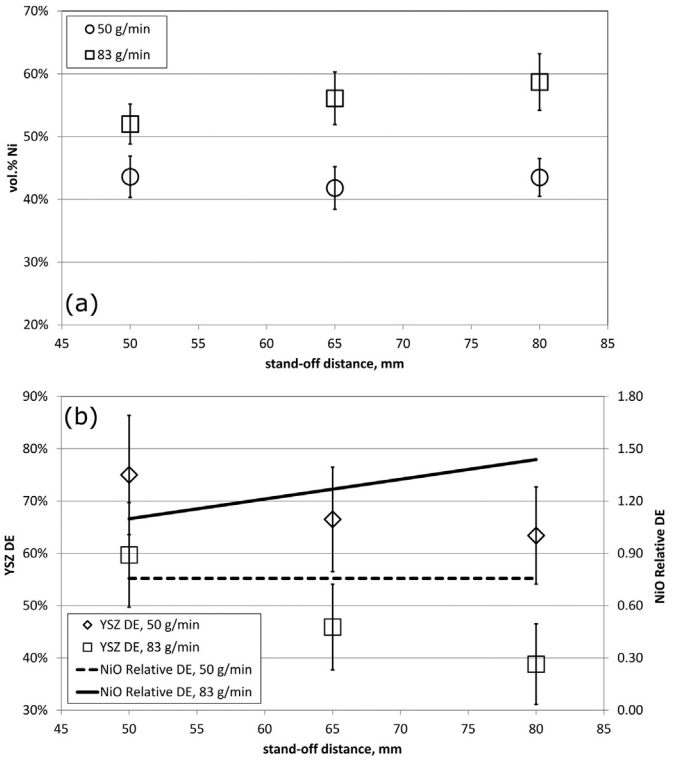

Fig. 3. (a) Nickel volume fraction relative to total solid volume of Ni and YSZ phases with increasing stand-off distance for two different suspension feed rates of 50 g min^{-1} and 83 g min^{-1}. (b) NiO DE relative to YSZ DE *right* and YSZ DE *left* over a range of stand-off distances. The plasma gas contains 60% N_2, balance Ar in both (a) and (b).

correspond to a composition of 50 vol.% Ni, relative to total solid volume, after reduction of NiO to Ni. The measured compositions of the deposited coatings were higher than 50 vol.% Ni for all conditions except for that of the shortest stand-off distance of 50 mm and highest N_2 content of 60%.

The deposition efficiencies of NiO and YSZ, at a stand-off distance of 50 mm, are shown in Fig. 2(b). The DE of the YSZ phase is significantly lower than that of the NiO phase for plasma gas compositions having 40% and 50% N_2, corresponding to torch powers of 76 kW and 89 kW, respectively. However, for a plasma gas composition of 60% N_2, corresponding to a torch power of 105 kW, the NiO DE and YSZ DE are similar. The lower YSZ DE, compared to that of NiO, at lower torch powers suggests that there is insufficient melting of the YSZ, resulting in poor adhesion upon impact with the substrate. As the N_2 content increases, both the total DE and YSZ DE relative to the NiO DE increase. Therefore, the desired composition of 50 vol.% Ni can be obtained by careful adjustment of the N_2 content in the plasma gas and stand-off distance for a given suspension flow rate.

3.1.2. *Effect of suspension mass flow rate*

The effect of suspension mass flow rate on deposition of the NiO and YSZ phases was assessed by fabricating coatings using two different suspension feed rates of 50 g min^{-1} and 83 g min^{-1}. Stand-off distances of 50 mm, 65 mm, and 80 mm were used, and the N_2 content of the plasma gas was fixed at 60%. For each of these conditions, Type F NiO was used. Fig. 3(a) shows the increase in Ni content at the shortest stand-off distance of 50 mm, from 44 vol.% ± 3 vol.% at 50 g min^{-1} to 52 vol.% ± 3 vol.% at 83 g min^{-1}. The difference in Ni content resulting from the different suspension feed rates increases as the stand-off distance increases, likely due to insufficient melting or re-solidification of YSZ at longer stand-off distances.

Fig. 3(b) shows the YSZ DE for both suspension feed rates of 50 g min^{-1} and 83 g min^{-1}. Also shown is the NiO DE relative to the YSZ DE, which does not change with stand-off distance at the lower suspension feed rate of 50 g min^{-1}, while it increases with stand-off distance at the higher suspension feed rate of 83 g min^{-1}. The NiO DE is therefore decreasing at the same rate with respect to stand-off distance as is the YSZ DE at the lower feed rate. However, at the higher feed rate, the YSZ DE is decreasing more quickly than the NiO DE with respect to increasing stand-off distance. This result is consistent with re-solidification of YSZ as the mean particle surface temperature decreases below its melting temperature of approximately 2700 °C.

The amount of water injected into the plasma increases with increasing suspension feed rate. The heat required to vaporize the increased water content is not available to treat the NiO and YSZ particles, resulting in cooler particle temperatures. This explanation is supported by Fig. 4, which shows cooler particle surface temperatures at higher suspension feed rates for a suspension of NiO (Type Std.) and YSZ particles without addition of carbon black. The mean particle surface temperatures for the 50 g min^{-1} and 83 g min^{-1} feed rates are 2850 °C ± 430 °C and 2660 °C ± 390 °C, respectively. Therefore, the mean particle surface temperature obtained with the lower flow rate of 50 g min^{-1} is greater than the melting temperature of YSZ, whereas the mean particle surface temperature obtained with the higher flow rate of 83 g min^{-1} is lower than the melting temperature of YSZ. Therefore, higher mass flow rates of aqueous suspensions may lead to NiO-rich coatings, if the water content is sufficient to prevent a significant fraction of the YSZ particles from being heated to their melting temperature.

3.1.3. *Effect of NiO particle size*

The size of the NiO particles in suspension affects the Ni content in the deposited coatings. Fig. 5 shows the vol.% Ni, relative to total

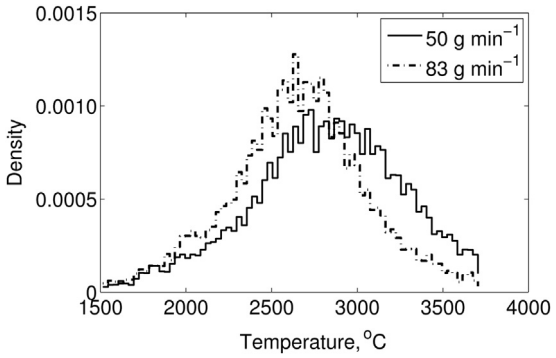

Fig. 4. Mean particle surface temperature for two different suspension feed rates of 50 g min^{-1} and 83 g min^{-1} at a stand-off distance of 50 mm. The plasma gas contained 60% N_2 for both suspension feed rates.

solid volume content of Ni and YSZ phases, in the deposited coatings for each NiO powder: Type A, Type F, and Type Std., as well as for mixtures of equal proportions of Type F and Type A and equal proportions of all three NiO types. All coatings in Fig. 5 were fabricated using Conditions B in Table 1. The smallest NiO particles in suspension, Type F, led to coatings having the lowest quantity of Ni, whereas coatings with the largest NiO particles in suspension, Type A and Type Std., have the highest quantity of Ni.

The larger NiO particles have a higher in-flight momentum and are more likely to penetrate the boundary layer that develops as the plasma gases are redirected at the substrate surface. The uncertainty captured in the error bars in Fig. 5 primarily accounts for the uncertainty associated with the mass increase of the metal substrate due to oxidation during both plasma spray deposition and during the pore-former removal step. However, uncertainty may also arise from different settling rates of the suspensions with differently sized NiO particles, leading to more or less Ni being delivered at the injection point. An effort was made to minimize uncertainty related to settling by constantly stirring the suspensions with a magnetic stir bar during spraying.

The mechanism responsible for larger NiO particles in suspension leading to larger NiO content in the deposited coatings is not clear. It is thought that the larger NiO particles have a larger momentum, if they are accelerated to the same velocity as smaller NiO particles at the location of the substrate, and therefore have a larger probability of penetrating the boundary layer that develops as plasma gases are redirected at the substrate surface.

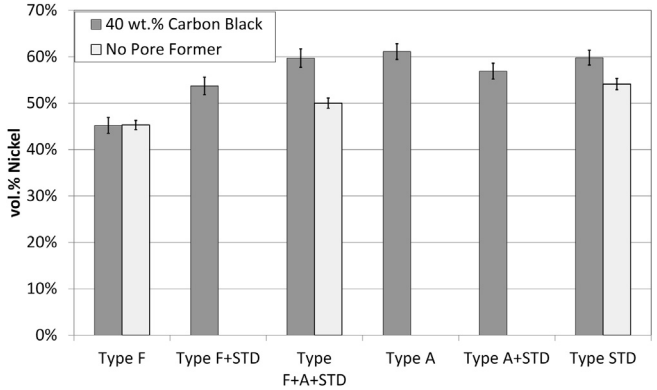

Fig. 5. Vol.% Ni, relative to total solid volume of Ni and YSZ phases, in Ni–YSZ coatings deposited directly onto metal supports using suspensions containing different NiO powders, with and without addition of carbon black as a sacrificial pore forming material.

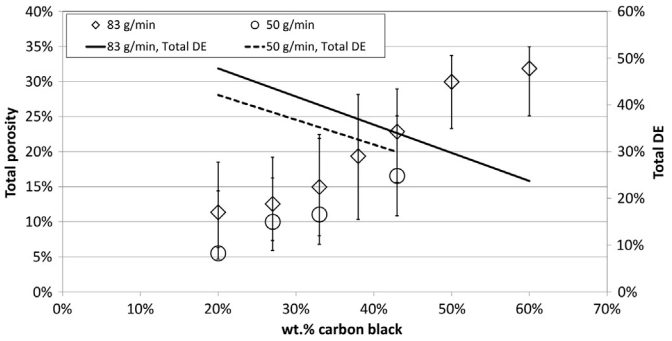

Fig. 6. Total porosity of Ni–YSZ coatings (after reduction of Type F NiO to Ni) with increasing wt.% of carbon black added to the suspension as a pore-forming material, for two suspension feed rates of 50 g min^{-1} and 83 g min^{-1}. Trend in deposition efficiency for both feedstock flow rates with increasing carbon black addition is also shown.

3.2. Total porosity

The open porosity of the anode should be sufficient so as to ensure negligible concentration polarization at the desired operating point. It is generally accepted that porosities between approximately 30% and 40% are required for high performance SOFC electrodes. For SOFC electrodes fabricated by plasma spraying, it is difficult to achieve porosities in this range, and the effect of porosity on electrochemical performance for electrode microstructures obtained by plasma spray methods is not well known.

Porosity is introduced to the anode through a number of different mechanisms. The anode is deposited as a composite of NiO and YSZ, which upon reduction of NiO to Ni results in a decrease in solid volume. Additional porosity results from partial melting of the NiO and YSZ particles, which traps pores as successive particles overlap [23], as well as through interlamellar and intralamellar cracks. Using Conditions C listed in Table 1, the total porosity was further increased through the addition of increasing amounts of carbon black added to the composite suspension. The carbon black was added as a sacrificial pore-forming material, which was removed after deposition by heating in air to 750 °C at 5 °C min^{-1} and holding for 2 h. Fig. 6 shows the increase in total porosity for increasing amounts of carbon black, using Type F NiO in the NiO–YSZ composite suspension. For carbon black additions of 60 wt.%, relative to suspended solids, a total porosity between 25% and 35% was obtained. Additions of carbon black below approximately 20 wt.% had little effect on the coating porosity.

The large uncertainty in the estimated total porosity is due to uncertainty attributed to gray-level thresholding and the ambiguity of pore-phase detection due to the large depth of field in an SEM. For thresholding, a heuristic approach was used such that two threshold values were estimated, each of which transforms all levels to either white or black, corresponding to the pore phase or solid phase, respectively. These two threshold values were obtained manually, by adjusting the threshold to values that appeared to represent the most reasonable minimum and maximum porosity values. The coating porosity was then expressed as the mean value between the heuristically determined minimum and maximum porosity values.

It is evident from the data presented in Fig. 6 that the total porosity and DE of the deposited coating depend on the flow rate of suspension injected into the plasma, with a higher flow rate corresponding to both higher total porosity and higher DE. The increase in porosity with feedstock flow rate is attributed to a larger degree of partial melting of the NiO and YSZ due to cooler plasma temperatures resulting from higher feedstock flow rate. The trade-off to the

increase in total porosity through increased addition of carbon black to the suspension, however, is the corresponding decrease in DE. Fig. 6 shows the decrease in DE from approximately 48%–23% with carbon black additions between 20 wt. % and 60 wt.%.

The variation in total porosity with the quantity of carbon black in suspension was not quantitatively evaluated for the remaining NiO sizes of Type A and Type Std., or for mixtures of these powders. However, a qualitative comparison is made for Type F NiO and for a mixture of equal amounts of Type A and Type Std., both with and without 40 wt.% carbon black added to the suspension, as shown in Fig. 7. Comparing Fig. 7(a) and (c), there are a larger number of micrometer sized pores when using the larger NiO particles in suspension. This difference is likely a result of partial melting of larger NiO particles. The particles trap voids upon stacking with each subsequent pass of the plasma gun. Conversely, the smaller Type F NiO particles are likely to be more completely melted, resulting in fewer trapped voids. The carbon black increases the coating porosity for both suspensions, as evident in Fig. 7(b) and (d).

3.3. Surface roughness

The surface roughness of the as-deposited NiO–YSZ coatings is affected by the stand-off distance between the torch nozzle exit and the substrate surface, as well as the in-flight droplet momentum. In general, the average surface roughness of the deposited coatings was found to decrease with increasing stand-off distance. However, in order to obtain the desired volume fraction of Ni in the coating, the stand-off distance was fixed at 50 mm. For the aqueous NiO–YSZ suspensions used in this study, in-flight droplet momentum was found to significantly affect the surface roughness of the deposited coatings.

The droplet momentum depends on both droplet density and droplet velocity. Fig. 8 shows the decrease in average surface roughness for coatings deposited using feedstock suspensions having larger NiO primary particle sizes. The coatings were fabricated using Conditions B in Table 1 and had a targeted thickness of 75 μm. The mechanism to which roughness formation is attributed is droplets having insufficient momentum normal to the substrate to penetrate the boundary layer that develops as plasma gases are deflected at the substrate surface [24]. Therefore, material that travels with the plasma gas, moving parallel to the substrate surface, deposits on surface asperities, leading to a buildup of clump-like surface features, as evident in Fig. 9. This hypothesis is supported by the decrease in surface roughness observed with increasing NiO particle size, due to the correspondingly larger magnitude of momentum of each droplet for suspensions containing larger NiO particles. Furthermore, a significant decrease in surface roughness is observed for feedstock suspensions not

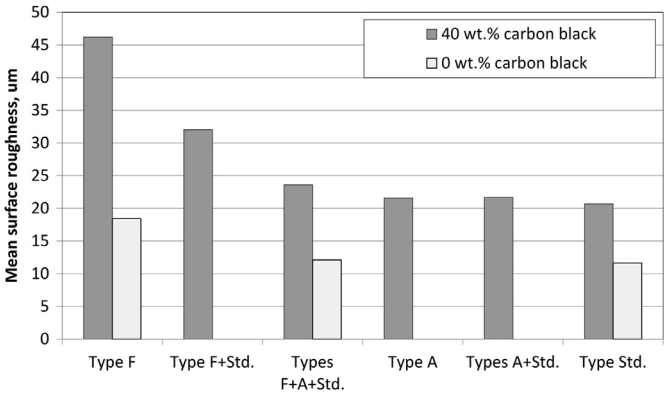

Fig. 8. Mean surface roughness for Ni–YSZ coatings deposited directly onto metal supports using suspensions containing different NiO powders, with and without the addition of carbon black as a sacrificial pore-forming material.

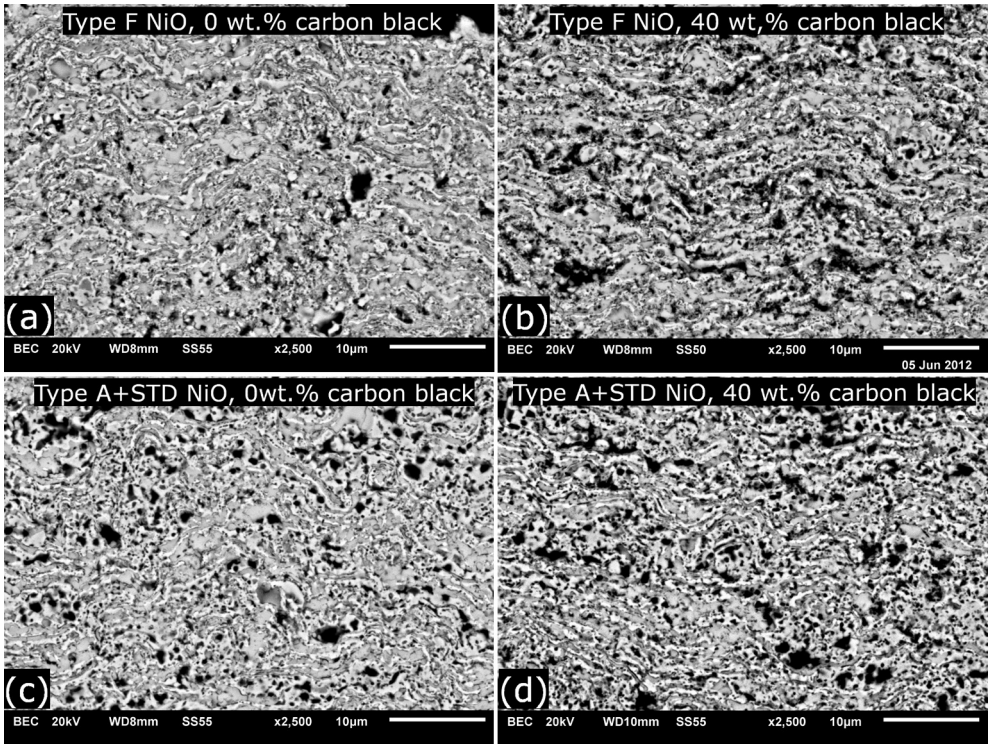

Fig. 7. Representative regions of Ni–YSZ coatings fabricated using Type F NiO powder (a) without carbon black and (b) with 40 wt.% carbon black added to the suspension. Representative regions of Ni–YSZ coatings fabricated using equal amounts of Type A and Type Std. NiO powder in (c) without carbon black and (d) with 40 wt.% carbon black added to the suspension.

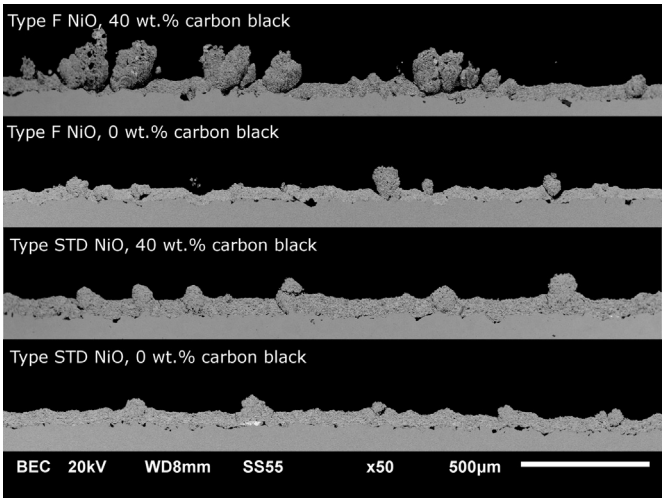

Fig. 9. Cross sections of coatings deposited using Type F NiO and Type Std. NiO, both with and without the addition of carbon black. The clump-like features contributing to high surface roughness are evident in each coating.

containing carbon black. The carbon black has a d_{50} of 0.6 µm by volume in suspension, as well as a low density (approximately 2 g cm^{-3}), which leads to a reduction in the magnitude of the momentum of each droplet. Therefore, coating surface roughness increases with the addition of carbon black to the suspension.

The surface roughness of the anode should be sufficiently low that defects do not form in the electrolyte during deposition. Plasma spraying is a line-of-sight deposition process, meaning that the electrolyte would not have uniform thickness at the locations of clump-like features, which are visible in Fig. 9. The surface roughness due to clump-like features that result from the build-up of material on surface asperities is dependent on the amount of material deposited. Therefore, the coating thickness should be limited to a value having an acceptable surface roughness. The critical thickness will in part depend on the surface roughness of the substrate (i.e. frequency and size of surface asperities), with lower substrate roughness leading to a larger critical thickness.

3.4. Fuel cell characterization

A fuel cell was fabricated for which the anode, electrolyte, and cathode were each deposited by plasma spray methods. The anode

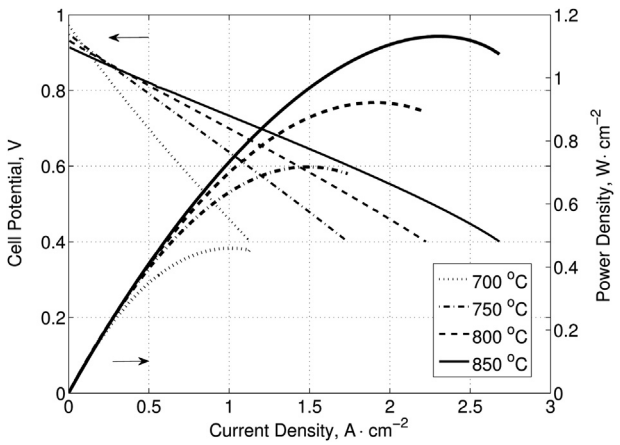

Fig. 10. Cell potential and power density as functions of current density at temperatures of 700 °C, 750 °C, 800 °C, and 850 °C. Anode fuel stream is humidified (≈3 mol.% H_2O) hydrogen at 400 sccm. Oxidant stream is air at 1000 sccm.

Table 2
Summary of performance parameters.

Temperature (°C)	Nernst potential (V)	OCV (V)	Peak power W cm^{-2}	Power at 0.7 V W cm^{-2}	R_s Ω cm^2	R_p Ω cm^2
850	1.094	0.914	1.13	0.832	0.095	0.079
800	1.102	0.931	0.923	0.700	0.135	0.092
750	1.111	0.948	0.718	0.555	0.194	0.113
700	1.119	0.972	0.460	0.348	0.272	0.182

was a bi-layer consisting of the surface-pore bridging layer (≈40 µm thick) deposited using dry-powder composite NiO–YSZ nanostructured agglomerate feedstock. The functional layer was fabricated by SPS using a composite NiO–YSZ suspension for which the NiO powder contained equal parts of NiO Type A and Type Std. powders (≈20 µm thick). Carbon black was added at 40 wt.% of total solid content as a sacrificial pore-forming agent. The electrolyte and cathode were deposited using SPS and conventional APS with YSZ and nanostructured LSCF-SDC agglomerated powder, respectively.

3.4.1. Electrochemical performance

Fig. 10 shows the cell potential and power density as functions of current density for temperatures from 700 °C to 850 °C. Performance parameters including the open circuit potential, power

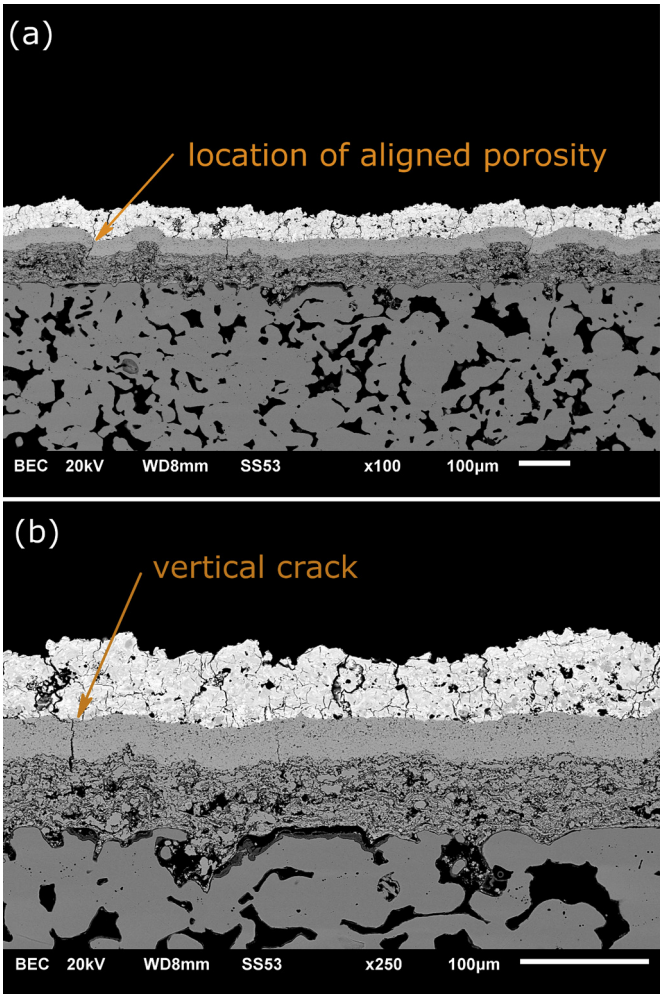

Fig. 11. Backscattered electron images of the cross section of the fabricated SOFC showing locations of (a) aligned porosity through the electrolyte formed at anode clump-like surface asperities and (b) vertical crack through the electrolyte.

density, and series and polarization resistances are summarized in Table 2. At 750 °C, the peak power density was 0.718 W cm^{-2}, and the power density at 0.7 V was 0.555 W cm^{-2}. It should be noted that the open circuit potential is significantly lower than the Nernst value for each temperature evaluated, suggesting that gas crossover occurred through defects in the electrolyte. For example, at 750 °C, the open circuit potential was 0.948 V, which is considerably less than the Nernst potential of 1.111 V. Therefore, the heat released during combustion of the fuel serves to raise the cell temperature above that measured by the thermocouple, which is positioned approximately 2 mm below the center of the cathode surface. This effect may be in part responsible for the high measured power densities (and correspondingly low series and polarization resistances). It was estimated that the actual average cell temperature may be as much as 50 °C higher than the furnace set point. This estimate was obtained by measuring the cell resistance at different fuel dilutions and comparing the change in the measured series resistance to the theoretical bulk resistance as a function of temperature, using Fig. 2 in Ref. [25] for the theoretical values.

3.4.2. Post-mortem analysis

Electrolyte defects leading to the observed loss in OCV include regions of aligned porosity [26] and vertical cracks [21] through the electrolyte, examples of which are shown in Fig. 11(a) and (b), respectively. Aligned porosity through the electrolyte forms at locations of anode surface defects. The anode bridging layer was fabricated using agglomerates in the −75 μm + 45 μm size fraction. Therefore, a partially melted agglomerate can comprise a significant portion of the ≈40 μm thick layer, leading to a stacking defect in subsequent layers. Therefore, care must be taken to minimize surface roughness of the layers upon which the electrolyte is deposited.

A backscattered electron image of the cross section of the fabricated cell after testing is shown in Fig. 12(a) for comparison to a representative bi-layer anode after fabrication in Fig. 12(b). The bi-layer anode in Fig. 12(b) was fabricated during the same spray runs as the anode for the cell in Fig. 12(a); however, aside from a heat treatment step at 600 °C in 25 vol.% H_2, balance N_2, it was not subjected to any further heat treatment. The coarsening of Ni in both the bridging layer and functional layer that occurred during electrochemical testing is apparent by comparing Fig. 12(a) and (b). While the degree of coarsening has not been quantified, a qualitative comparison between these two images shows that the degree of coarsening is large, and has occurred over approximately 60 h at furnace temperatures between 700 °C and 850 °C.

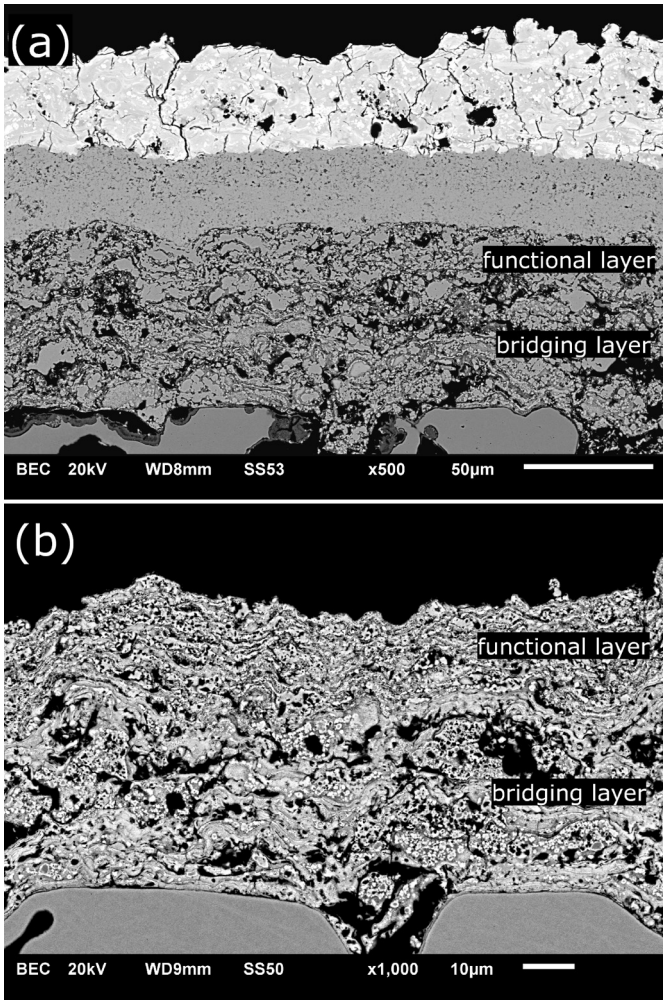

Fig. 12. Backscattered electron images of the cross section of (a) the fabricated SOFC after electrochemical testing and (b) a representative bi-layer anode showing both the bridging layer and the functional layer. The bi-layer anode in (b) has been heat treated at 600 °C for 4 h in 25 vol.% H_2, balance N_2, to reduce the NiO to Ni.

4. Conclusions

The effects of plasma gas composition, stand-off distance, NiO particle size, and feed rate of suspension on the composition of Ni–YSZ coatings were evaluated using composite aqueous suspensions of NiO and YSZ. Increasing the stand-off distance and decreasing the N_2 content in the plasma gas lead to increasing Ni content relative to YSZ. The N_2 content within the plasma must be sufficient to melt the YSZ particles, which in this work was 60 vol.%, balance Ar. However, the stand-off distance must be sufficiently short that the YSZ particles do not re-solidify as the plasma temperature cools at longer stand-off distances, which leads to a lower probability of adhesion on impact. The Ni content of the deposited coatings is also affected by the feed rate of the injected suspension. As the feed rate increases, the heat required to vaporize the water causes cooler particle surface temperatures, on average, which leads to insufficient melting of YSZ. Furthermore, higher Ni concentrations are obtained in coatings for which larger NiO particles were used. The increased in-flight momentum of the larger NiO particles leads to a higher probability that they will penetrate the boundary layer that develops as the plasma gas is redirected at the substrate surface.

The total porosity of the coatings may be increased through the addition of sacrificial pore-forming agents to the suspension feedstock. Carbon black added to the suspensions in quantities greater than 20 wt.% led to an increase in total porosity from less than 12% to 33% when added at 60 wt.%. There is, however, both a corresponding decrease in DE of both NiO and YSZ and an increase in surface roughness as the carbon black content increases. The surface roughness may be minimized by increasing the droplet momentum, by increasing the size of the NiO particles in suspension, and by decreasing the carbon black content.

A fuel cell was fabricated having a bi-layer anode with functional layer deposited by SPS. The peak power densities at 750 °C and 850 °C were 0.718 W cm^{-2} and 1.13 W cm^{-2}, respectively. However, as indicated by the low open circuit potentials measured compared to the corresponding Nernst potentials, gas crossover through defects in the electrolyte are likely leading to combustion, which raises the actual temperature of the fuel cell. This results in lower series and polarization resistances than if the gas crossover was not occurring. The performance obtained is promising; however, further work into minimizing the occurrence of electrolyte defects and improving the anode functional layer microstructure are required, particularly related to Ni coarsening.

Acknowledgments

The authors gratefully acknowledge financial support from the Natural Sciences and Engineering Research Council (NSERC) of Canada, as well as from the Solid Oxide Fuel Cells Canada Strategic Research Network sponsored by NSERC and other sponsors listed at www.sofccanada.com. The authors wish to thank Michael Marr and Jeffrey Harris for their help making the electrolyte and cathode layers as well as the Centre for Advanced Coating Technologies (CACT) at the University of Toronto for use of their facilities. Michael Marr also provided the method to estimate elevated cell temperatures during cell testing. Donations of the gasket material by Flexitallic and of carbon black by Cancarb Ltd. are also greatly appreciated.

References

[1] R. Hui, Z. Wang, O. Kesler, L. Rose, J. Jankovic, S. Yick, R. Maric, D. Ghosh, Journal of Power Sources 170 (2007) 308–323.
[2] P. Bance, N. Brandon, B. Girvan, P. Holbeche, S. ODea, B. Steele, Journal of Power Sources 131 (2004) 86–90.
[3] N.P. Brandon, A. Blake, D. Corcoran, D. Cumming, A. Duckett, K. El-Koury, D. Haigh, C. Kidd, R. Leah, G. Lewis, C. Matthews, N. Maynard, N. Oishi, T. McColm, R. Trezona, A. Selcuk, M. Schmidt, L. Verdugo, Journal of Fuel Cell Science and Technology 1 (2004) 61–65.
[4] Y. Matus, L. De Jonghe, C. Jacobson, S. Visco, Solid State Ionics 176 (2005) 443–449.
[5] M. Lang, R. Henne, S. Schaper, G. Schiller, Journal of Thermal Spray Technology 10 (2001) 618–625.
[6] G. Schiller, R. Henne, M. Lang, M. Müller, Materials Science Forum 426–432 (2003) 2539–2544.
[7] D. Stöver, D. Hathiramani, R. Vaßen, R.J. Damani, Surface and Coatings Technology 201 (2006) 2002–2005.
[8] R. Vaßen, D. Hathiramani, J. Mertens, V. Haanappel, I. Vinke, Surface and Coatings Technology 202 (2007) 499–508.
[9] X. Ma, H. Zhang, J. Dai, J. Roth, R. Hui, T. Xiao, D. Reisner, Journal of Thermal Spray Technology 14 (2005) 61–66.
[10] R. Hui, J.O. Berghaus, C. Decès-Petit, W. Qu, S. Yick, J.-G. Legoux, C. Moreau, Journal of Power Sources 191 (2009) 371–376.
[11] R. Lima, B. Marple, Journal of Thermal Spray Technology 16 (2007) 40–63.
[12] C. Metcalfe, J. Harris, J. Kuhn, M. Marr, O. Kesler, Journal of Thermal Spray Technology (2013), http://dx.doi.org/10.1007/s11666-013-9884-0.
[13] D. Goberman, Y. Sohn, L. Shaw, E. Jordan, M. Gell, Acta Materialia 50 (2002) 1141–1152.
[14] P. Fauchais, R. Etchart-Salas, C. Delbos, M. Tognonvi, V. Rat, J. Coudert, T. Chartier, Journal of Physics D: Applied Physics 40 (2007) 2394–2406.
[15] H. Kaßner, R. Siegert, D. Hathiramani, R. Vaßen, D. Stöver, Journal of Thermal Spray Technology 17 (2008) 115–123.
[16] R. Vaßen, H. Kaßner, G. Mauer, D. Stöver, Journal of Thermal Spray Technology 19 (2010) 219–225.
[17] P. Fauchais, V. Rat, C. Delbos, J. Coudert, T. Chartier, L. Bianchi, IEEE Transactions on Plasma Science 33 (2005) 920–930.
[18] O. Marchand, P. Bertrand, J. Mougin, C. Comminges, M.-P. Planche, G. Bertrand, Surface and Coatings Technology 205 (2010) 993–998.
[19] Y. Wang, J.-G. Legoux, R. Neagu, S. Hui, B. Marple, Journal of Thermal Spray Technology 21 (2012) 7–15.
[20] R. Rampon, O. Marchand, C. Filiatre, G. Bertrand, Surface and Coatings Technology 202 (2008) 4337–4342.
[21] M. Marr, O. Kesler, Surface and Coatings Technology 216 (2013) 289–296.
[22] J. Harris, C. Metcalfe, M. Marr, J. Kuhn, O. Kesler, Journal of Power Sources 239 (2013) 234–243.
[23] J. Ilavsky, A.J. Allen, G.G. Long, S. Krueger, C.C. Berndt, H. Herman, Journal of the American Ceramic Society 80 (1997) 733–742.
[24] J. Oberste Berghaus, J.-G. Legoux, C. Moreau, F. Tarasi, T. Chráska, Journal of Thermal Spray Technology 17 (2008) 91–104.
[25] J.W. Fergus, Journal of Power Sources 162 (2006) 30–40.
[26] D. Waldbillig, O. Kesler, Journal of Power Sources 191 (2009) 320–329.